metals

MDPI

Article

Microstructural Modification by Large Pre-Deformation and Post-Aging to Improve Properties in Al-Mg-Li Alloy

Zeyu Zheng [1], Peipei Ma [2,*], Longhui Chen [1] and Chunhui Liu [1,3,*]

[1] State Key Laboratory of Precision Manufacturing for Extreme Service Performance, Light Alloy Research Institute, Central South University, Changsha 410083, China
[2] School of Physics, Central South University, Changsha 410083, China
[3] School of Mechanical and Electrical Engineering, Central South University, Changsha 410083, China
* Correspondence: mapeipei@csu.edu.cn (P.M.); chunhuiliu@csu.edu.cn (C.L.)

Abstract: Al-Mg-Li alloy is an ideal lightweight structural material for aerospace applications due to its low density, high specific strength, and excellent low-temperature performance. This study examines the mechanical properties and microstructural evolution of Al-Mg-Li alloy subjected to cryogenic and room temperature cold rolling, which induces large plastic deformation. Compared with room temperature rolling, cryogenic rolling significantly reduces surface cavity formation, thereby enhancing the alloy's rolling surface quality. After cryogenic rolling by 80% and subsequent natural aging, the yield strength of artificially aged Al-Mg-Li alloy reaches 560 MPa, delivering a 60% increase compared to the traditional T6 state with a slight reduction in elongation from 6.5% to 4.6%. The specific strength achieves 2.23 × 10^5 N·m/kg, outperforming conventional Al-Cu-Li and 7xxx-series Al alloys. The depth of intergranular corrosion decreases from 100 μm to 10 μm, demonstrating excellent corrosion resistance enabled by the new method. Transmission electron microscopy reveals that finely distributed δ′ (Al_3Li) is the primary strengthening phase, with high-density dislocations further enhancing strength. However, coarsening of δ′ (from ~2.9 nm to >6 nm) induced by ensuing artificial aging results in coplanar slip and reduced elongation. Lowering the post-aging temperature inhibits δ′ coarsening, thereby improving both strength and elongation. Our results provide valuable insights into optimizing the properties of Al-Mg-Li alloys for advanced lightweight applications.

Keywords: Al-Mg-Li alloy; cryogenic rolling; artificial aging; mechanical properties; microstructural evolution

check for updates

Academic Editors: Anders E. W. Jarfors, Murat Tiryakioglu and Martin Leitner

Received: 26 January 2025
Revised: 2 March 2025
Accepted: 4 March 2025
Published: 6 March 2025

Citation: Zheng, Z.; Ma, P.; Chen, L.; Liu, C. Microstructural Modification by Large Pre-Deformation and Post-Aging to Improve Properties in Al-Mg-Li Alloy. *Metals* **2025**, *15*, 290. https://doi.org/10.3390/met15030290

Copyright: © 2025 by the authors. Licensee MDPI, Basel, Switzerland. This article is an open access article distributed under the terms and conditions of the Creative Commons Attribution (CC BY) license (https://creativecommons.org/licenses/by/4.0/).

1. Introduction

With the intensification of the global energy crisis and environmental challenges, energy conservation and emission reduction have emerged as critical development priorities for modern society. Material lightweighting technology has gained significant attention as a core approach to achieving these goals [1–3]. Aluminum–magnesium–lithium (Al-Mg-Li) alloy [4], recognized for its exceptionally low density (2.47 g/cm^3) within the aluminum alloy family, holds great promise for weight reduction, particularly in rail transportation and aerospace applications [5,6]. Despite these advantages, the mechanical performance of aged Al-Mg-Li alloys, including strength and elongation, remains inferior to widely used high-strength aluminum alloys, such as the 7xxx and 2xxx series [7–9]. This performance gap significantly limits its application in high-performance fields [10–12]. Consequently, developing effective strengthening strategies to enhance the mechanical properties of Al-Mg-Li alloys is essential for expanding their use in advanced engineering applications.

The Al-Mg-Li alloys have been extensively studied to enhance their properties by optimizing alloy composition, refining preparation and processing techniques, and improving heat treatment methods. Betsofen et al. [13] reported that in Al-Mg-Li alloys prepared via smelting and hot extrusion, the cast structure predominantly consists of α-Al, while the extruded and T6-treated structures are primarily composed of δ′ (Al_3Li) and S1 (Al_2MgLi) phases. These phases, with their characteristic $L1_2$ structure, tend to promote coplanar slip, adversely impacting the alloy's plasticity [14]. Shi et al. observed that increasing the Mg content refines the grain size of cast Al-Mg-Li alloys but also accelerates δ′ precipitation and coarsening during aging, thereby affecting precipitation strengthening and alloy strength. C.Q. Li et al. [15] demonstrated that after solutionizing at 350 °C, followed by a T4 aging treatment, the α-Mg and AlLi phases in the cast Al-Mg-Li alloy dissolve and transform into a single β-Li matrix, resulting in a homogeneous body-centered cubic (BCC) solid solution. This transformation significantly enhances both the mechanical properties and corrosion resistance of the alloy. Li et al. [16] proposed a retrogression and re-aging (RRA) treatment to regulate the size of precipitated phases, maintaining the good plasticity of aged alloys. Xiao et al. [17,18] showed that the EAT (EARA + EAA) treatment of cold-rolled Al-Mg-Li alloys alters the morphology and distribution of precipitates, significantly improving mechanical properties. In addition to improving the heat treatment method, microalloying is another effective approach for enhancing the performance of Al-Mg-Li alloys. For instance, Yang demonstrated that adding Sc and Zr to the 1420 alloy promotes the formation of Al_3(Sc, Zr) particles, which not only stabilize the microstructure but also delay the coarsening of Al_3Li and δ′-PFZ precipitates [19]. This results in a significant enhancement in the alloy's strength, surpassing 300 MPa. Thus, the primary strategy for strengthening Al-Mg-Li alloys involves controlling the distribution and size of key precipitated phases. While microalloying and adjustments to the heat treatment system can effectively increase the strength of these alloys beyond 300 MPa, they still lag behind the performance of widely used alloys such as 2195 and 7075 [20]. To bridge this gap, new methods are needed to further enhance alloy performance. One promising technique is the application of large pre-deformation combined with a subsequent aging process. This method works by regulating the interactions between dislocations and precipitates, resulting in a significant improvement in the alloy's mechanical properties [21–23]. For example, Liu et al. [21] increased the mechanical properties of the AA2219 alloy by enhancing dislocation density and stability, achieving a 130 MPa strength improvement after 80% pre-deformation and aging at 150 °C. Similarly, Chen et al. [22] reported a 60–140 MPa strength increase in the Al-Mg-Si alloy through pre-deformation and 180 °C aging. These studies demonstrate the potential of this strategy for industrial applications and the performance optimization of Al-Mg-Li alloys.

However, the poor plasticity of Al-Mg-Li alloys makes them prone to cracking during large cold rolling deformation [24–26], which is also a challenge observed in Al-Zn-Mg-Cu alloys [27]. Zhu et al. [28] addressed this issue using cryogenic rolling to achieve 80% pre-deformation in Al-Zn-Mg-Cu alloys, followed by creep aging at 120 °C, improving strength by 110 MPa and enhancing corrosion resistance in 7xxx series alloys. Studies on 2xxx and 6xxx series alloys [29–31] further confirm that cryogenic technology improves plastic deformation limits, microstructure, and overall performance after deformation.

In this study, cryogenic and room temperature (RT) rolling processes were employed to prepare Al-Mg-Li alloys. The effects of large pre-deformation combined with subsequent aging on the microstructure and mechanical properties of the alloy were systematically investigated using advanced characterization techniques such as TEM, EBSD, and XRD, alongside comprehensive mechanical property testing. The results indicate that cryogenic

rolling followed by natural aging yields Al-Mg-Li alloys with optimal comprehensive performance, balancing strength, plasticity, and corrosion resistance. While cryogenic rolling improves material properties, its potential impact on manufacturing costs must be weighed against its performance benefits. This research provides innovative technical insights for expanding the application of Al-Mg-Li alloys in lightweight structural materials, offering promising solutions for next-generation engineering demands.

2. Materials and Methods

The material used in this study is an aluminum–magnesium–lithium alloy (1420 Al-Li alloy) with a nominal composition of Al-5.1%Mg-1.7%Li-0.1%Sc-0.03%Zr-0.4%Zn. After solution treatment at 450 °C for 30 min, the alloy was rolled at room temperature and cryogenic conditions with a rolling reduction of 80%. Following rolling, the alloy underwent natural aging to peak hardness and artificial aging at 125 °C, 145 °C, and 165 °C in an oil bath furnace. Figure 1 presents a schematic diagram of the heat treatment process employed in this study.

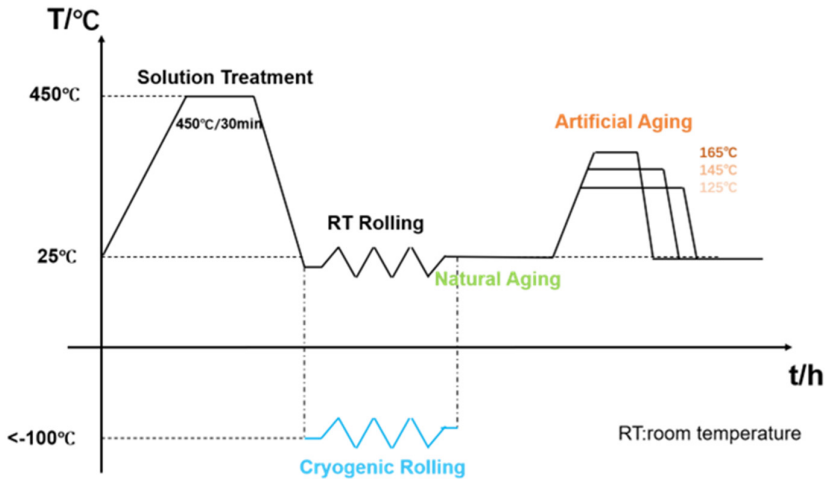


Figure 1. Thermo-mechanical schedules for preparation of Al-Mg-Li alloy.

The surface morphology of the Al-Mg-Li alloy under different rolling temperatures was analyzed using a scanning electron microscope (Helios 5 CX). The macroscopic hardness changes during natural and artificial aging after rolling were measured using an HDX-100TM/LCD Vickers hardness tester. Hardness measurements were performed with a square cone diamond indenter under a 9.8 N load for 10 s. The quasi-static tensile properties of the alloy at room temperature and at each aging peak state were evaluated using an MTS universal testing machine at a strain rate of 2 mm/min, with the average of at least five independent measurements recorded for each set of hardness and tensile data. Intergranular corrosion tests followed the GB/T 41653-2022 standard [32], using samples of 25 mm × 40 mm. Corrosion depth was measured after immersion in a 30 g/L hydrochloric acid solution for 12 h. The dislocation and precipitate distribution of the alloy in its initial rolled state and at the peak-aged state were observed using a field emission scanning transmission electron microscope (Talos F200X manufactured by Thermofisher, USA). TEM samples were prepared using an electrolytic double-spray thinning instrument and thinned with a 3:7 nitric acid–methanol solution (HNO_3:CH_3OH) at approximately −25 °C.

3. Results

3.1. Surface Morphology and Pore Distribution of Aluminum–Magnesium–Lithium Alloy Rolled at Room and Cryogenic Temperatures

The W-state aluminum–magnesium–lithium alloy was rolled with an 80% reduction at room temperature and under cryogenic conditions, immersed in liquid nitrogen. As shown in Figure 2a,b, the plate rolled at room temperature exhibited severe cracking and continuous edge fractures, whereas the surface of the plate rolled at cryogenic temperature remained relatively intact. To further analyze the surface morphology and investigate the cracking mechanisms of the alloy, the cracked-edge sections of the plates were observed using scanning electron microscopy (SEM), with the results presented in Figure 2c–h. Micron-scale pores were observed on the alloy surface under both rolling conditions, but the number of pores was significantly reduced after cryogenic rolling. Analysis revealed that, within the same edge area, the pores' density after cryogenic rolling was less than 10% of that after room temperature rolling.

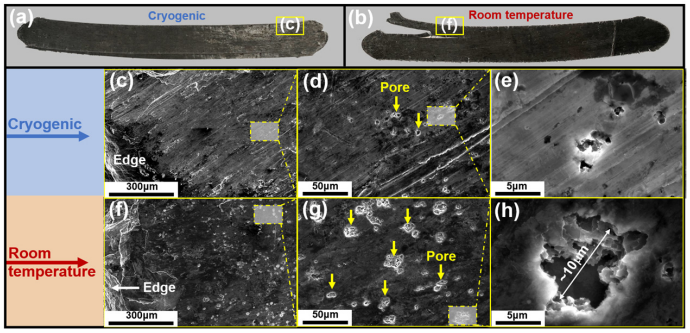


Figure 2. SEM images of the surface morphology of the largely pre-deformed Al-Mg-Li alloy. (**a**,**b**) Macroscopic appearance of the Al-Mg-Li alloy prepared by cryogenic rolling and RT rolling; (**c**–**e**) surface of the alloy after cryogenic rolling; and (**f**–**h**) surface of the alloy after RT rolling.

Additionally, Figure 3 presents SEM images of the cavity density at different distances from the crack center along the crack direction of the alloy surface after room temperature rolling in the same field of view. The results indicate that the cavity density is significantly higher near the crack center, with a concentration within a 3 mm radius from the crack center. Specifically, the pore counts in the observation areas at distances of 0, 1, 2, and 3 mm from the crack center were 510, 400, 200, and 85, respectively, showing a reduction of over 80% in pore density within the 3 mm radius of the crack center.

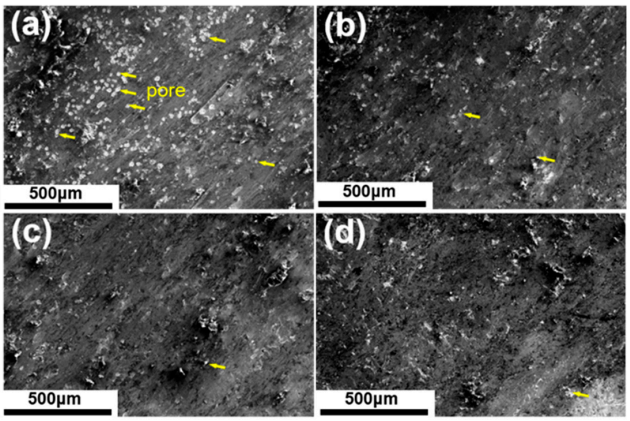


Figure 3. SEM images of different positions of largely pre-deformed Al-Mg-Li alloy. (**a**) 1 mm from crack; (**b**) 2 mm from crack; (**c**) 3 mm from crack; and (**d**) 4 mm from crack.

3.2. Mechanical Properties and Microstructural Evolution of Al-Mg-Li Alloy with Large Pre-Deformation

Figure 4 illustrates the hardness changes of two groups of rolled Al-Mg-Li alloys during subsequent natural aging and artificial aging at different temperatures. As shown in Figure 4a, both liquid nitrogen-rolled and room temperature-rolled alloys exhibit significant natural aging hardening behavior. The room temperature-rolled alloy shows a rapid increase in hardness during the initial stage of natural aging, reaching a peak of 178 HV after 5–6 days, and stabilizing after approximately one week. In contrast, the liquid nitrogen-rolled sample reaches a slightly lower peak hardness of 175 HV. This indicates that large deformation enables the precipitation of strengthening phases during natural aging, and increases the hardness of the alloy. However, the thermal effects of room temperature rolling accelerate the precipitation of the secondary phase, leading to a higher hardness compared to cryogenic rolling. Figure 4b–d show the artificial aging hardening curves of the two alloy groups at 125 °C, 145 °C, and 165 °C. The alloys exhibit a similar aging hardening behavior across these temperatures: an initial rapid drop in hardness to approximately 150 HV, followed by a gradual increase to a peak hardness of 170–175 HV, and then stabilized. The two rolled alloys exhibit similar aging kinetics. As the temperature increases, the peak hardness is reached at a faster rate. For example, alloys aged at 125 °C and 145 °C achieve peak hardness (175 HV) after 16 and 24 h, respectively, while those aged at 165 °C reach peak hardness (170 HV) in just 4 h. Cryogenic-rolled alloys follow a similar trend but show a slightly lower final peak hardness, approximately 5 HV lower than their room temperature-rolled counterparts.

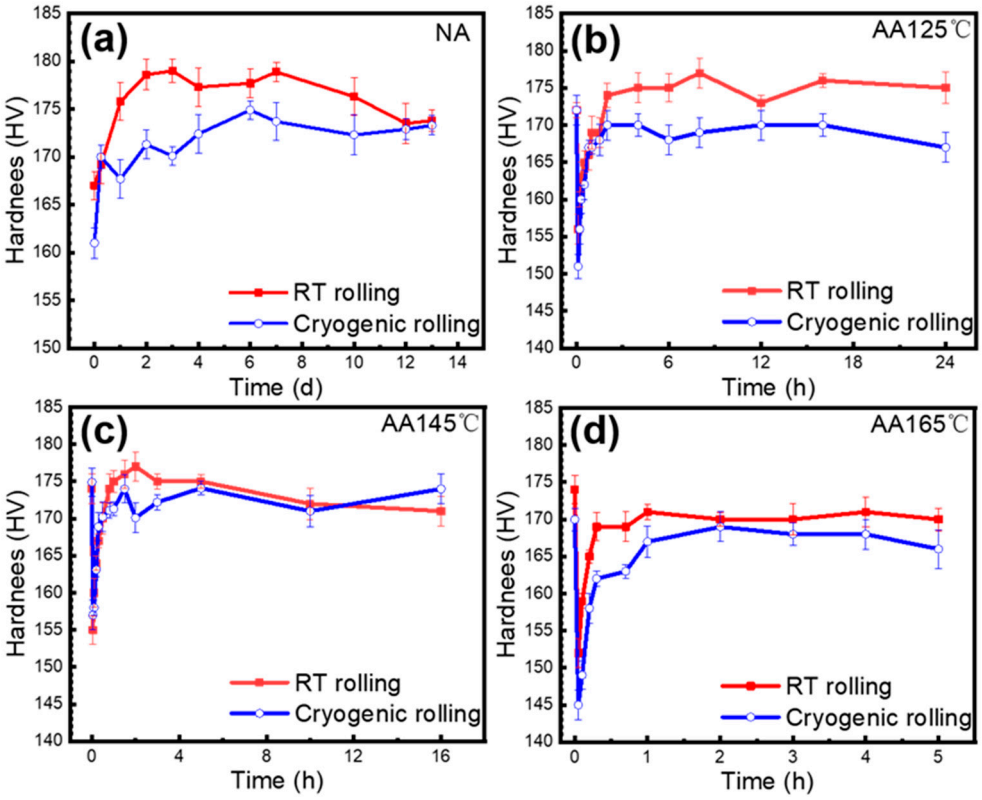


Figure 4. Subsequent age hardening curves of largely pre-deformed Al-Mg-Li alloy. (**a**) Natural aging (NA) process and (**b**–**d**) artificial aging (AA) process at 125 °C, 145 °C, and 165 °C.

The uniaxial tensile properties of peak-aged Al-Mg-Li alloys after natural aging and artificial aging at different temperatures were tested and compared with those of conventionally T6-treated samples. Additionally, the results from samples rolled at liquid nitrogen

and room temperature were analyzed to evaluate the impact of different rolling conditions. The T6-treated alloy exhibited a relatively low strength, with a yield strength of only 350 MPa. However, after 80% pre-deformation and subsequent low-temperature aging, the alloy's strength improved significantly. As shown in Figure 5a, the yield strength of the alloy exceeded 500 MPa, representing a more than 40% increase compared to the T6 state, although plasticity slightly decreased. Figure 5b shows that alloys rolled at cryogenic temperatures achieved similar results, with yield strengths exceeding 500 MPa after aging. The final yield strengths of (CR-NA Cryogenic rolling combined with subsequent natural aging), CR-125 °C, and CR-145 °C samples were 560 MPa, 510 MPa, and 500 MPa, respectively, with the CR-NA alloy maintaining an elongation of approximately 4%. However, the yield strength decreased after aging at 165 °C, likely due to excessive thermal recovery. It is noteworthy that after natural aging, the cryogenically rolled alloy showed a 40 MPa higher strength and 1.5% greater elongation compared to the room temperature-rolled alloy. This suggests that the cryogenic environment facilitates a synergistic enhancement of both strength and plasticity in aluminum–magnesium–lithium alloys subjected to significant pre-deformation and natural aging. In summary, aluminum–magnesium–lithium alloys subjected to 80% cryogenic rolling followed by natural aging achieved a peak yield strength of 560 MPa, about 60% higher than the T6 state (~350 MPa), with elongation reduced from 6.5% to 4.6%. The 1420 aluminum alloy, with a density of 2.47 g/cm^3, is the lightest aluminum alloy. Specific strength, defined as the ratio of a material's yield strength to its density (σ/ρ), is a key parameter for evaluating materials in lightweight structural applications. Using this calculation, the specific strength of the 1420 alloy is determined to be 2.23 $\times$ 10^5 N·m/kg, significantly higher than that of conventional and high-strength 7-series aluminum alloys (~1.9 $\times$ 10^5 N·m/kg). This value highlights the alloy's exceptional strength-to-weight ratio, making it an ideal choice for applications that require both high strength and low density.

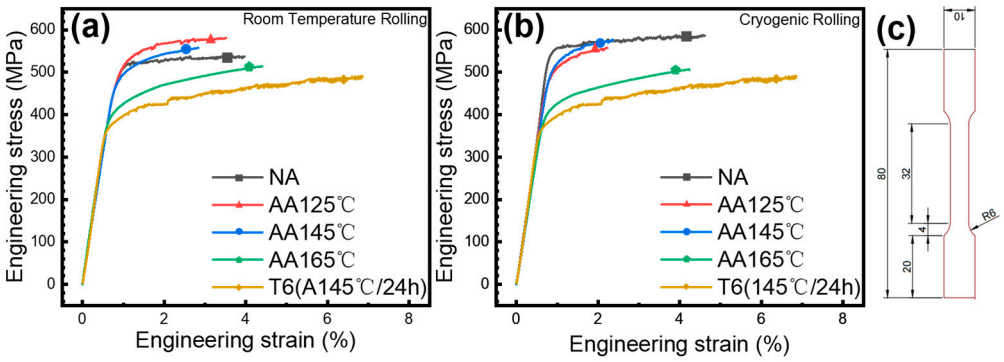


Figure 5. Tensile curves of largely pre-deformed and peak-aged Al-Mg-Li alloy. (**a**) Room temperature-rolled (RTR) alloy and (**b**) cryogenic temperature-rolled (CR) alloy. (**c**) Dimension of tensile specimen.

Electron backscatter diffraction (EBSD) analysis was conducted on the T4-state sample and the cryogenic temperature-rolled sample, with the results shown in Figure 6. The analysis reveals that the Al-Mg-Li alloy in the T4 state exhibits relatively intact elongated grain morphology, while cryogenic rolling significantly disrupts the grain structure.

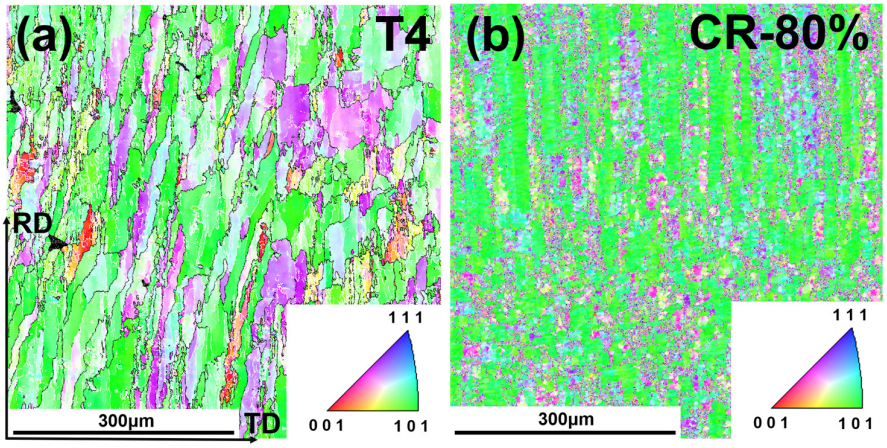


Figure 6. EBSD-IPF images of Al-Mg-Li alloy in different states. (**a**) T4; (**b**) as CR80%.

Notably, the W-state alloy exhibits pronounced texture characteristics (Figure 7a), with pole figure analysis identifying S{123}<634>, Brass{110}<112>, and Copper{112}<111> as the dominant texture types—typical deformation textures. After 80% pre-deformation, the material's texture intensity further increases (Figure 7b). This pronounced deformation texture likely enhances material strength through the mechanism of texture strengthening.

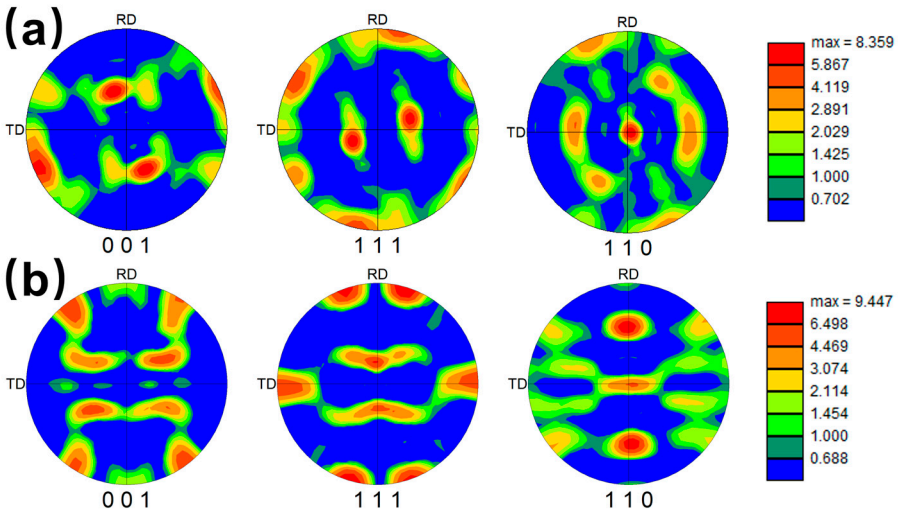


Figure 7. EBSD-PF images of Al-Mg-Li alloy in different states. (**a**) T4; (**b**) cold-rolled by 80%.

Subsequent microstructural characterization was performed using transmission electron microscopy (TEM) for the key groups, as shown in Figure 8a–c. The TEM bright-field images depict the Al-Mg-Li alloy in its initial state after 80% cryogenic rolling and subsequent aging at 125 °C and 165 °C. The results reveal that 80% cryogenic rolling induces a high density of dislocations within the aluminum–magnesium–lithium alloy matrix, with pronounced dislocation entanglement. Furthermore, after prolonged low-temperature aging or short-term high-temperature aging, the dislocation structure remains largely unchanged, consistently exhibiting significant dislocation entanglement. These findings highlight that dislocation strengthening is a critical microscopic mechanism contributing to the superior mechanical properties of high-strength Al-Mg-Li alloys achieved through large deformation and subsequent aging.

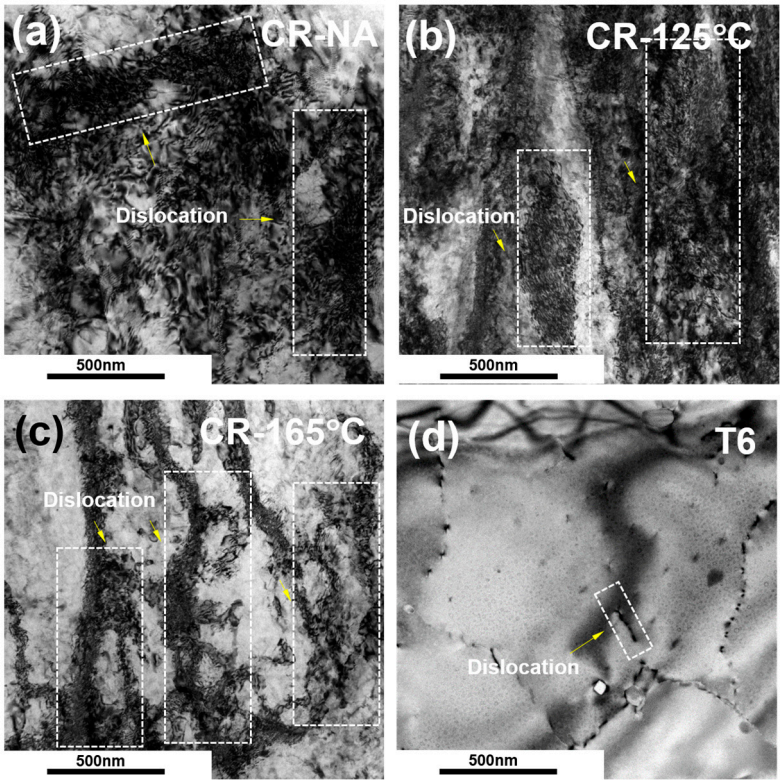


Figure 8. Dislocation morphology of T6 state and largely pre-deformed Al-Mg-Li alloy after different aging treatments. (**a**) CR; (**b**) CR-125 °C; (**c**) CR-165 °C; and (**d**) T6.

Figure 9a presents the TEM dark-field image of the alloy in the T6 state (145 °C-16 h), while Figure 9b–d display the TEM dark-field images of the alloy after 80% cryogenic rolling, natural aging, and aging at 125 °C and 165 °C, respectively. As the primary strengthening phase, the spherical Al_3Li phase was analyzed for its density and size in the <001> orientation. The bright spots in the images represent precipitates. Figure 9e shows the high-resolution image of the Al_3Li precipitate at the peak natural aging state after 80% cryogenic rolling. Figure 9f illustrates a schematic of this structure. The blue spheres represent aluminum atoms, and the brown spheres represent lithium atoms, forming a typical $L1_2$ structure. Due to their atomic number differences, the heavier aluminum appears brighter in the image, while the lithium appears as dark spots. The T6 alloy exhibits a significant number of dispersed Al_3Li precipitates, with an average size of approximately 18 nm. In contrast, large pre-deformation enables the formation of finer Al_3Li precipitates during subsequent natural aging at 25 °C. These precipitates are uniformly distributed, with an average size of about 3 nm. During artificial aging, thermodynamic effects increase the density and size of precipitates, with average sizes reaching 6 nm and 9 nm after aging at 125 °C and 165 °C, respectively, as shown in Figure 10. Precipitation strengthening, with Al_3Li as the primary phase, represents another fundamental mechanism for enhancing the strength of aluminum–magnesium–lithium alloys via large pre-deformation and aging. However, as a semi-coherent phase, excessively large Al_3Li precipitates may promote coplanar slip, compromising alloy ductility. Thus, achieving fine, densely distributed Al_3Li precipitates during natural aging is critical for maximizing strength while retaining sufficient ductility.

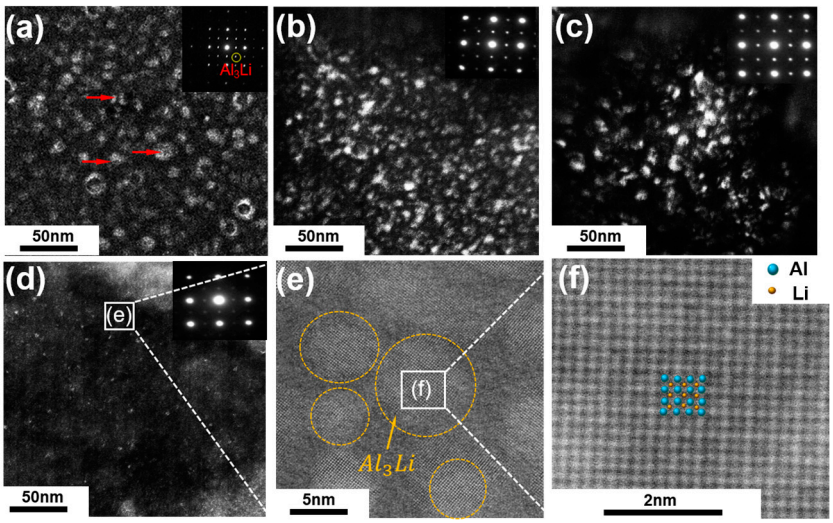


Figure 9. TEM and high-resolution HADDF images of Al_3Li precipitated phase in different states of largely pre-deformed Al-Mg-Li alloy. (**a**) T6; (**b**) CR-125 °C; (**c**) CR-165 °C; (**d**) CR-NA; (**e**) magnified section of (**d**); and (**f**) schematic diagram of Al_3Li atomic structure.

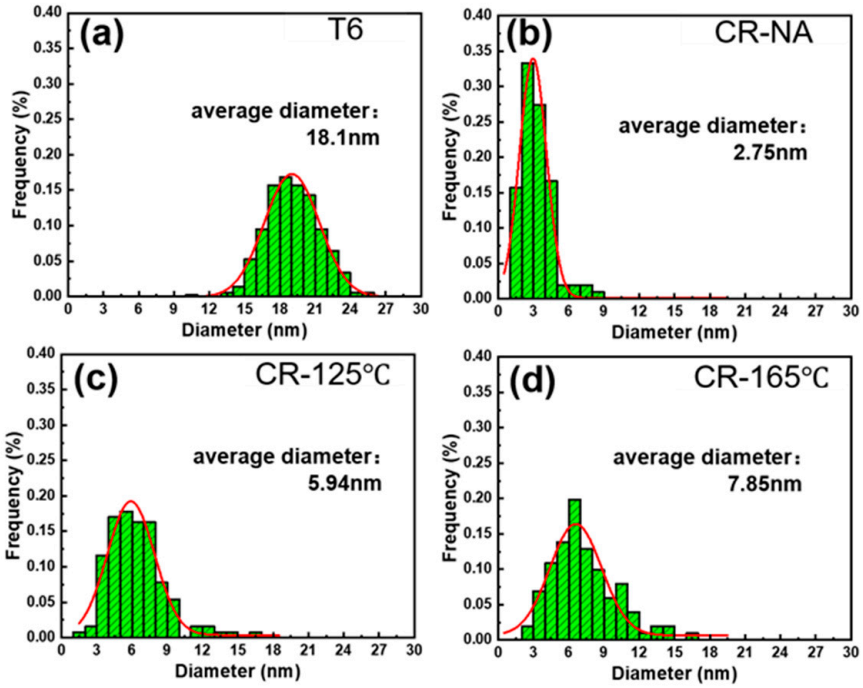


Figure 10. Statistical diagram of precipitation phases of Al-Mg-Li alloy in different states. (**a**) T6; (**b**) CR-NA; (**c**) CR-125 °C; and (**d**) CR-165 °C.

3.3. Intergranular Corrosion Properties of Large Pre-Deformation and Aging Al-Mg-Li Alloy

Aluminum–magnesium–lithium alloys hold significant potential for weight reduction applications due to their exceptionally low density. However, the high chemical activity of lithium in the alloy leads to poorer corrosion resistance compared to conventional magnesium alloys. Current mainstream methods for enhancing the corrosion resistance of aluminum–magnesium–lithium alloys include shot peening and composite coatings; both of which typically require additional processing steps after alloy preparation [33,34]. In contrast, large pre-deformation combined with the subsequent natural aging treatment significantly improves both the mechanical properties and corrosion resistance of the alloy. As illustrated in Figure 11, the average depth of intergranular corrosion in conventional T6 samples is approximately 100 microns, with the deepest corrosion reaching up to

125 microns. In comparison, CR-NA samples exhibit an average corrosion depth of only about 10 microns, and no corrosion is observed in certain areas. According to GB/T 41653-2022, intergranular corrosion resistance is classified based on maximum corrosion depth: ≤10 microns (Grade 1), 10–30 microns (Grade 2), 30–100 microns (Grade 3), 100–300 microns (Grade 4), and >300 microns (Grade 5). Our results indicate that the conventional T6 alloy falls into Grade 4, whereas the CR-NA sample achieves Grade 1, demonstrating significantly improved intergranular corrosion resistance. Results highlight the dual benefits of the large cryo-deformation and natural aging process in enhancing both the strength and durability of aluminum–magnesium–lithium alloys.

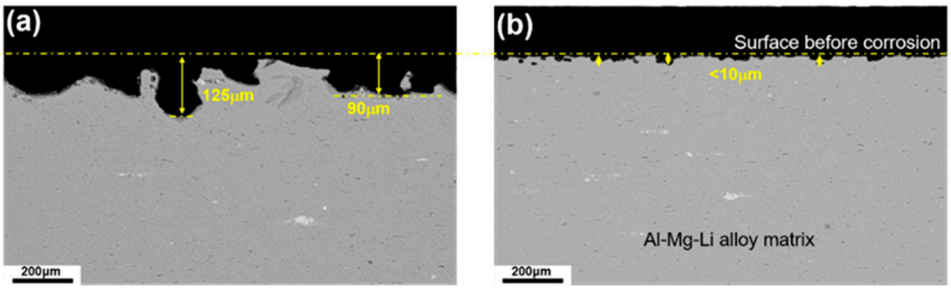


Figure 11. SEM images of intergranular corrosion depth of Al-Mg-Li alloy in different states. (**a**) T6 and (**b**) CR-NA.

4. Discussion

4.1. Liquid Nitrogen Ambient Temperature Suppresses Surface Pore Formation in Aluminum–Magnesium–Lithium Alloy

As illustrated in Figure 2, the surface of the Al-Mg-Li alloy after rolling exhibits micron-sized holes, whose distribution and size are significantly influenced by the rolling temperature. Under room temperature rolling conditions, the alloy surface contains a large number of holes, with an average size of approximately 10 microns. In contrast, rolling at liquid nitrogen ambient temperature drastically reduces the number of surface holes to just 1/10 of those formed under room temperature conditions, with most holes measuring less than 5 microns—roughly half the size of those formed at room temperature. Given that all other external conditions were consistent between the two rolling processes, it can be inferred that the rolling ambient temperature is the primary factor affecting the distribution and size of surface holes in the alloy.

In addition, as shown in Figure 12, observations of edge cracks in the room temperature-rolled samples revealed that the initiation point of the crack was a surface hole on the alloy, with a high density of larger holes distributed near the crack. Along the direction of the crack, the density of holes gradually decreases, and moving away from the crack centerline, the number of holes significantly diminishes with increasing distance. These findings indicate that surface holes formed during rolling not only initiate cracks but also contribute to their propagation, making them a critical factor that limits the deformation capacity of the Al-Mg-Li alloy under room temperature rolling. In contrast, rolling at liquid nitrogen ambient temperature effectively suppresses the formation of surface holes. This may be due to the extreme low-temperature effects on the material during the cryogenic treatment of liquid nitrogen, resulting in changes in its molecular structure, the rearrangement of its lattice structure, and the release of residual stresses inside the material [35,36], thereby increasing the deformation limit of the alloy and enhancing its rolling performance.

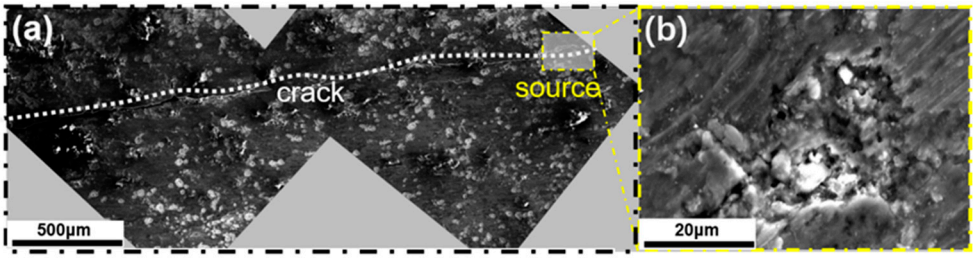


Figure 12. SEM images of edge cracks in room temperature-rolled alloy. (**a**) Crack propagation path and (**b**) magnified image of initial cavity.

4.2. Strength Contribution of Dislocation Density

In this study, the strength of the Al-Mg-Li alloy prepared through large pre-deformation combined with a subsequent natural aging treatment increased by 210 MPa compared to the conventional T6-aged state. Owing to the inherently low density of the material, the alloy also achieved an exceptionally high specific strength. The enhancement in alloy strength is primarily attributed to dislocation strengthening and precipitation strengthening. The contributions of these two mechanisms to the overall strength improvement can be estimated using the widely adopted dislocation strengthening calculation method and the precipitation strengthening formula proposed by Nie and Muddle et al. [37].

In order to further study the changes in dislocation density in pre-deformation combined with subsequent natural aging and the conventional T6 state Al-Mg-Li alloy and their role in alloy strengthening, the improved Williamson–Hall method was used to calculate the dislocation density (ρ) in the aluminum alloy sample from the synchrotron XRD profile (Figure 13) [38]. The dislocation density ρ can be obtained by fitting the function of the diffraction peak broadening and its relationship:

$$\Delta K = \frac{D}{0.9} + \left(\frac{2\pi M^2}{b^2}\right)\cdot\rho^{\frac{1}{2}}\cdot K^2\overline{C} + \beta W_{hkl} + O(K^4\overline{C}^2) \quad (1)$$

where $\overline{C}$ is the average contrast factor $\{hkl\}$ for each specific plane, D is the grain size, M is the Wilkens arrangement parameter, b is the Burgers vector (0.286 nm for aluminum), ρ is the dislocation density, β is the fracture probability, W_{hkl} is the scaling factor for the fault-induced peak broadening at the $\{hkl\}$ reflection, and h, k, and l are the Miller indices for each peak. High-resolution 2θ scans are used to measure the effect of extended age time on the broadening of the diffraction peaks. Each diffraction peak is fitted with a pseudo-Voigt function to calculate the full width at half maximum. ΔK is the broadening FWHM in reciprocal space and is given by:

$$\Delta K = \frac{\cos\theta(\Delta 2\theta)}{\lambda} \quad (2)$$

where θ is the diffraction angle, $\Delta 2\theta$ is the half-height width of the diffraction peak at θ, λ is the wavelength of the X-ray, and K is the diffraction vector, which is defined as:

$$K = \frac{2\sin\theta}{\lambda} \quad (3)$$

The difference in the average contrast factor ($\overline{C}$) of different diffraction peaks is used to explain the anisotropy of broadening [39,40]:

$$\overline{C} = \overline{C}_{h00}\left(1 - q\left(\frac{h^2k^2 + h^2l^2 + k^2l^2}{(h^2 + k^2 + l^2)^2}\right)\right) \quad (4)$$

where $\overline{C}_{h00}$ and q represent different broadening anisotropies and vary depending on the dislocation type (edge or screw). Six reflection peaks (111), (200), (220), (311), (222), and (400) are recorded for each line profile. Then ρ is carefully determined to have the best linear fit between ΔK and $K^2\overline{C}$.

Finally, the calculated dislocation density data are substituted into the dislocation strengthening formula:

$$\Delta_{\sigma_\rho} = \alpha M G b \rho^{\frac{1}{2}} \quad (5)$$

Among them, α, M, G, and b are all constants related to the basic properties of the material, so the specific value of dislocation strengthening can be calculated. According to Figure 13, the diffraction angles and full width at half maximum (FWHM) values for the T6 and CR-NA samples are as follows: for the T6 sample, the diffraction angles are [38.375, 44.5, 78.025] with corresponding FWHM values of [0.098523, 0.168229, 0.156851], while for the CR-NA sample, the diffraction angles are [38.375, 44.625, 65, 78.05] with FWHM values of [0.1919, 0.22211, 0.4308, 0.35215]. Based on these data, the dislocation densities of the two alloys can be fitted accordingly. The final calculation results show that the dislocation density of the T6 aluminum–magnesium–lithium alloy is $7.18 \times 10^{13}\,m^{-2}$, while the dislocation density of the natural aging sample after deep cold rolling increases significantly to $7.15 \times 10^{14}\,m^{-2}$, which is an order of magnitude different from the two. By substituting the dislocation density data into the dislocation strengthening formula, it is calculated that the difference in dislocation strengthening contribution between the conventional T6 state and the large cryo-deformation combined with the subsequent natural aging treatment of the aluminum–magnesium–lithium alloy is approximately 177 MPa. This indicates that during the process of large pre-deformation combined with subsequent natural aging, the dislocation strengthening contributes 85% of the total strength increase of the alloy (which is a total increase of 210 MPa in strength).

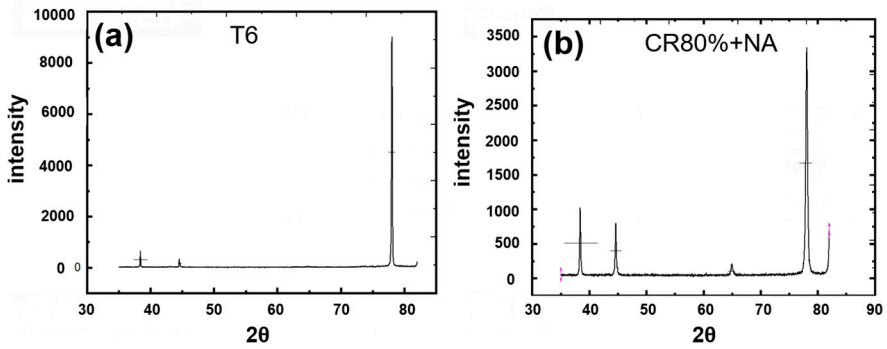


Figure 13. Synchrotron radiation XRD patterns. (**a**) T6 and (**b**) CR-NA.

4.3. The Evolution of the δ′ Phase During Aging and Its Impact on Mechanical Properties

Existing studies generally believe that an Al-Mg-Li alloy is a typical aging material, and its high strength is mainly enhanced by the fine Al_3Li precipitate phase uniformly dispersed after aging treatment. The aging response of the alloy is generally the result of the response between dislocations and Al_3Li precipitate phases. When the size of Al_3Li particles is below the critical value, the precipitate phase is easily cut by dislocations. Since the matrix of the Al-Mg-Li alloy is a disordered or short-range family solid solution, the full dislocation in the matrix has a Burgers vector of a0/2-⟨110⟩, while in the Al_3Li precipitate phase, the Burgers vector type of the full dislocation is a0-⟨110⟩. This indicates that there is one full dislocation in the Al_3Li precipitate phase instead of two full dislocations in the matrix. Therefore, the slip of such dislocations has a strengthening effect on the alloy. After the dislocation shears the precipitate phase, the original grid structure is destroyed,

and antiphase boundaries (APBs) are formed in the precipitate phase. The formation of APBs represents the resistance that the dislocation movement must overcome, further improving the strength of the alloy. However, after the first dislocation slides through the Al_3Li phase, the resistance of subsequent dislocations sliding on the same slip surface will be significantly reduced. This phenomenon may lead to the occurrence of coplanar slip, which will have an adverse effect on the plasticity of aluminum–lithium alloys.

Generally, in the under-aged state, small-diameter precipitates are easily sheared by dislocations; in the peak aging state, the size and volume fraction of Al_3Li particles increase, resulting in greater resistance for dislocation movement, while the dislocation gap is significantly reduced, and the strength of the alloy is significantly improved due to the fine and uniform distribution of precipitates. When the aging time is further extended, the particle size of the Al_3Li phase exceeds the critical size that can be cut by dislocations, and the precipitation mechanism is transformed into bypassing the Al_3Li phase through the Orowan mechanism. According to Figure 14, in the aluminum–magnesium–lithium alloy prepared by large pre-deformation combined with the subsequent aging process in this study, the main size of the precipitate phase is significantly smaller than the size of the precipitate phase in the conventional T6 state alloy in the peak aging state.

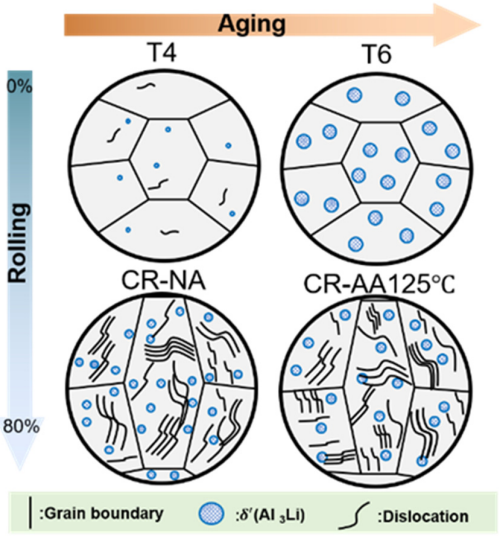


Figure 14. Schematic diagram of microstructure evolution of Al-Mg-Li alloy prepared by large pre-deformation combined with aging process.

The further comparison of the precipitate phase size of subsequent natural aging and low-temperature artificial aging found that in the matrix with high-density dislocation distribution, the Al_3Li precipitate phase in the alloy treated with subsequent natural aging is smaller in size and more densely distributed. The evolution law of this δ′ phase shows that the aluminum–magnesium–lithium alloy prepared by deep cold large pre-deformation and subsequent natural aging can achieve the best strengthening effect through the synergistic effect of dislocation strengthening and precipitation strengthening mechanisms, thereby obtaining an aluminum–magnesium–lithium alloy with excellent mechanical properties.

5. Conclusions

We have proposed a novel approach that integrates a cryogenic rolling pre-treatment to introduce high-density dislocations with subsequent natural aging, significantly enhancing the mechanical properties and microstructural evolution of aluminum–magnesium–lithium alloys. This cryogenic rolling process effectively suppresses the formation of surface cavities during room temperature rolling, leading to fewer and smaller voids, which improve the

alloy's rolling ability. The resulting alloy exhibits a substantial increase in yield strength (~560 MPa) and specific strength (2.23 × 10^5 N·m/kg), surpassing conventional high-strength aluminum alloys such as the 2xxx and 7xxx series, albeit with a 30% reduction in elongation. Furthermore, the alloy demonstrates significantly improved intergranular corrosion resistance, with the corrosion depth reduced to just 10% of that observed in conventional T6 alloys. Overall, this method offers a promising strategy for enhancing both the strength and corrosion resistance of aluminum–magnesium–lithium alloys, presenting significant potential for lightweight structural applications and providing new insights for the design of other age-hardenable metal alloys.

Author Contributions: Conceptualization, P.M. and C.L.; methodology, P.M.; validation, L.C.; formal analysis, P.M.; investigation, Z.Z.; resources, C.L.; data curation, Z.Z., L.C. and C.L.; writing—original draft, Z.Z. and L.C.; writing—review and editing, P.M. and C.L. All authors have read and agreed to the published version of the manuscript.

Funding: This research was funded by the National Natural Science Foundation of China, grant number 52305441.

Data Availability Statement: The original contributions presented in this study are included in the article. Further inquiries can be directed to the corresponding authors.

Conflicts of Interest: The authors declare no conflict of interest.

References

1. Braga, D.F.; Tavares, S.M.O.; Da Silva, L.F.; Moreira, P.M.G.P.; De Castro, P.M. Advanced design for lightweight structures: Review and prospects. *Prog. Aerosp. Sci.* **2014**, *69*, 29–39. [CrossRef]
2. Li, S.S.; Yue, X.; Li, Q.Y.; Peng, H.L.; Dong, B.X.; Liu, T.S.; Yang, H.Y.; Fan, J.; Shu, S.L.; Jiang, Q.C.; et al. Development and applications of aluminum alloys for aerospace industry. *J. Mater. Res. Technol.* **2023**, *27*, 944–983. [CrossRef]
3. Singh, J.; Srivastawa, K.; Jana, S.; Dixit, C.; Ravichandran, S. Advancements in lightweight materials for aerospace structures: A comprehensive review. *Acceleron Aerosp. J.* **2024**, *2*, 173–183. [CrossRef]
4. Furukawa, M.; Berbon, P.B.; Langdon, T.G.; Horita, Z.; Nemoto, M.; Tsenev, N.K.; Valiev, R.Z. Age hardening and the potential for superplasticity in a fine-grained Al-Mg-Li-Zr alloy. *Metall. Mater. Trans. A* **1998**, *29*, 169–177. [CrossRef]
5. Starke, E.A.; Sanders, T.H.; Palmer, I.G. New approaches to alloy development in the Al-Li system. *JOM* **1981**, *33*, 24–33. [CrossRef]
6. Rioja, R.J.; Warren, C.J.; Goodyear, M.D.; Kulak, M.; Bray, G.H. Al-Li alloys for lower wings and horizontal stabilizer applications. In *Materials Science Forum*; Trans Tech Publications Ltd.: Bäch, Switzerland, 1997; Volume 242, pp. 255–262.
7. Rodgers, B.I.; Prangnell, P.B. Quantification of the influence of increased pre-stretching on microstructure-strength relationships in the Al–Cu–Li alloy AA2195. *Acta Mater.* **2016**, *108*, 55–67. [CrossRef]
8. Zhou, B.; Liu, B.; Zhang, S. The advancement of 7xxx series aluminum alloys for aircraft structures: A review. *Metals* **2021**, *11*, 718. [CrossRef]
9. Lyu, F.; Li, Y.; Huang, X.; Shi, Z.; Zeng, Y.; Lin, J. An investigation of creep age forming of AA7B04 stiffened plates: Experiment and FE modelling. *J. Manuf. Process.* **2019**, *37*, 232–241. [CrossRef]
10. Wang, Z.C.; Prangnell, P.B. Microstructure refinement and mechanical properties of severely deformed Al–Mg–Li alloys. *Mater. Sci. Eng. A* **2002**, *328*, 87–97. [CrossRef]
11. Ye, L.; Liu, X.; Tang, J.; Liu, S.; Zhang, Y. Ostwald ripening and stability of precipitates during two successive overaging in an Al-Mg-Li alloy. *Mater. Lett.* **2021**, *291*, 129616. [CrossRef]
12. Matsumoto, H.; Watanabe, S.; Hanada, S. Fabrication of pure Al/Mg–Li alloy clad plate and its mechanical properties. *J. Mater. Process. Technol.* **2005**, *169*, 9–15. [CrossRef]
13. Betsofen, S.Y.; Antipov, V.V.; Knyazev, M.I. Al–Cu–Li and Al–Mg–Li alloys: Phase composition, texture, and anisotropy of mechanical properties. *Russ. Metall. (Met.)* **2016**, *2016*, 326–341. [CrossRef]
14. Shi, C.; Wu, G.; Zhang, L.; Zhang, X.; Sun, J.; Zhang, J. Microstructures and mechanical properties of ultralight cast Al-3Li-XMg-0.1 Zr alloys. *Mater. Charact.* **2020**, *170*, 110698. [CrossRef]
15. Li, C.Q.; Liu, X.; Dong, L.J.; Shi, B.Q.; Tang, S.; Dong, Y.; Zhang, Z.R. Simultaneously improved mechanical strength and corrosion resistance of Mg-Li-Al alloy by solid solution treatment. *Mater. Lett.* **2021**, *301*, 130305. [CrossRef]

16. Li, Y.; Meng, F.; Zheng, W.; Wang, Y. Small angle X-ray scattering study of the strengthen mechanism of Al–Mg–Li alloy during retrogression and reaging treatment. *J. Alloys Compd.* **2010**, *503*, 291–293. [CrossRef]
17. Xiao, H.; Jiang, S.; Zhang, K.; Jia, Y.; Shi, C.; Lu, Z.; Jiang, J. Optimizing the microstructure and mechanical properties of a cold-rolled Al–Mg–Li alloy via electropulsing assisted recrystallization annealing and ageing. *J. Alloys Compd.* **2020**, *814*, 152257. [CrossRef]
18. Xiao, H.; Lu, Z.; Zhang, K.; Jiang, S.; Shi, C. Achieving outstanding combination of strength and ductility of the Al-Mg-Li alloy by cold rolling combined with electropulsing assisted treatment. *Mater. Des.* **2020**, *186*, 108279. [CrossRef]
19. Wang, Y.; Liu, H.; Ma, X.; Wu, R.; Sun, J.; Hou, L.; Zhang, J.; Li, X.; Zhang, M. Effects of Sc and Zr on microstructure and properties of 1420 aluminum alloy. *Mater. Charact.* **2019**, *154*, 241–247. [CrossRef]
20. Liu, C.; He, J.; Feng, Z.; Ma, P.; Zhan, L. Integrating reversion ageing and forming of high-strength Al alloys: Principles and theoretical basis. *Int. J. Mach. Tools Manuf.* **2024**, *194*, 104091. [CrossRef]
21. Liu, C.; Yang, J.; Ma, P.; Ma, Z.; Zhan, L.; Chen, K.; Huang, M.; Li, J.; Li, Z. Large creep formability and strength–ductility synergy enabled by engineering dislocations in aluminum alloys. *Int. J. Plast.* **2020**, *134*, 102774. [CrossRef]
22. Chen, K.; Liu, C.; Ma, P.; Yang, J.; Zhan, L.; Huang, M.; Hu, J. Enhancing creep formability and comprehensive property in Al–Mg–Si alloy by combinatorial pre-ageing and large pre-deformation. *Mater. Sci. Eng. A* **2021**, *826*, 141967. [CrossRef]
23. Chen, L.; Liu, C.; Ma, P.; Yang, J.; Zhan, L.; Huang, M. Strong in-plane anisotropy of creep ageing behavior in largely pre-deformed Al-Cu alloy: Experiments and constitutive modeling. *Int. J. Plast.* **2021**, *152*, 103245. [CrossRef]
24. Wang, Y.; Zhang, Z.; Wu, R.; Sun, J.; Jiao, Y.; Hou, L.; Zhang, J.; Li, X.; Zhang, M. Ambient-temperature mechanical properties of isochronally aged 1420-Sc-Zr aluminum alloy. *Mater. Sci. Eng. A* **2019**, *745*, 411–419. [CrossRef]
25. Xiao, R.; Zhang, X. Problems and issues in laser beam welding of aluminum–lithium alloys. *J. Manuf. Process.* **2014**, *16*, 166–175. [CrossRef]
26. Zhu, Y.; Poplawsky, J.D.; Li, S.; Unocic, R.R.; Bland, L.G.; Taylor, C.D.; Locke, J.S.; Marquis, E.A.; Frankel, G.S. Localized corrosion at nm-scale hardening precipitates in Al-Cu-Li alloys. *Acta Mater.* **2020**, *189*, 204–213. [CrossRef]
27. Jeshvaghani, R.A.; Emami, M.; Shahverdi, H.R.; Hadavi, S.M.M. Effects of time and temperature on the creep forming of 7075 aluminum alloy: Springback and mechanical properties. *Mater. Sci. Eng. A* **2011**, *528*, 8795–8799. [CrossRef]
28. Zhu, H.; Ma, P.; Liu, C.; He, J.; Yang, J.; Chen, L.; Huang, L.; Zhan, L. Effect of cryogenic pre-deformation on the stress relaxation response and mechanical/corrosion properties in Al–Zn–Mg–Cu alloy. *J. Mater. Res. Technol.* **2022**, *20*, 3471–3484. [CrossRef]
29. Roven, H.J.; Starke, E.A., Jr.; Sødahl, Ø.; Hjelen, J. Effects of texture on delamination behavior of a 8090-type Al-Li alloy at cryogenic and room temperature. *Scr. Metall. Mater.* **1990**, *24*, 421–426. [CrossRef]
30. Panigrahi, S.K.; Jayaganthan, R. A study on the mechanical properties of cryorolled Al–Mg–Si alloy. *Mater. Sci. Eng. A* **2008**, *480*, 299–305. [CrossRef]
31. Xu, Z.; Roven, H.J.; Jia, Z. Mechanical properties and surface characteristics of an AA6060 alloy strained in tension at cryogenic and room temperature. *Mater. Sci. Eng. A* **2015**, *648*, 350–358. [CrossRef]
32. *GB/T 41653-2022*; Technical Committee 183 on Steel of Standardization Administration of China. Standardization Administration of the People's Republic of China: Beijing, China, 2022.
33. Kuang, Q.; Wang, R.; Peng, C.; Cai, Z.; Feng, Y.; Wang, X. Influence of aging treatment on the microstructure, mechanical properties and corrosion behavior of spray deposited Al-Mg-Li-Sc-Zr alloy. *J. Alloys Compd.* **2021**, *881*, 160664. [CrossRef]
34. Xu, X.J.; Hao, M.; Chen, J.Z.; He, W.W.; Li, G.A.; Li, K.X.; Jiao, C.; Zhong, X.L.; Moore, K.L.; Zhou, X.R.; et al. Role of constituent intermetallic phases and precipitates in initiation and propagation of intergranular corrosion of an Al-Li-Cu-Mg alloy. *Corros. Sci.* **2022**, *201*, 110294. [CrossRef]
35. Wang, Y.; Zuo, J.; Xu, C.; Liu, W.; Li, D.; Wang, G.; Tang, G.; Geng, L. Deformation behavior of pure aluminum at room and cryogenic temperatures. *J. Mater. Res. Technol.* **2024**, *31*, 2355–2366. [CrossRef]
36. Yang, Q.Y.; Zhou, Y.L.; Tan, Y.B.; Xiang, S.; Ma, M.; Zhao, F. Effects of microstructure, texture evolution and strengthening mechanisms on mechanical properties of 3003 aluminum alloy during cryogenic rolling. *J. Alloys Compd.* **2021**, *884*, 161135. [CrossRef]
37. Nie, J.F.; Muddle, B.C. Microstructural design of high-strength aluminum alloys. *J. Phase Equilibria* **1998**, *19*, 543–551. [CrossRef]
38. Ungár, T. Characterization of nanocrystalline materials by X-ray line profile analysis. *J. Mater. Sci.* **2007**, *42*, 1584–1593. [CrossRef]
39. Ungár, T.; Dragomir, I.; Révész, Á.; Borbély, A. The contrast factors of dislocations in cubic crystals: The dislocation model of strain anisotropy in practice. *J. Appl. Crystallogr.* **1999**, *32*, 992–1002. [CrossRef]
40. Ungár, T.; Ott, S.; Sanders, P.G.; Borbély, A.; Weertman, J.R. Dislocations, grain size and planar faults in nanostructured copper determined by high resolution X-ray diffraction and a new procedure of peak profile analysis. *Acta Mater.* **1998**, *46*, 3693–3699. [CrossRef]

Disclaimer/Publisher's Note: The statements, opinions and data contained in all publications are solely those of the individual author(s) and contributor(s) and not of MDPI and/or the editor(s). MDPI and/or the editor(s) disclaim responsibility for any injury to people or property resulting from any ideas, methods, instructions or products referred to in the content.